This article has been accepted for inclusion in a future issue of this journal. Content is final as presented, with the exception of pagination.

Compact Triple-Band Active Switchable Bandpass Filter With Enhanced Passband Isolation

Ruofeng Xu, Wenhan Wu, Xianglin Kong, Jun Wang, *Member, IEEE*, Yunze Hu, Guoqing Pan, and Lei Zhao, *Senior Member, IEEE*

***Abstract*—In this letter, a compact bandpass filter (BPF) is proposed, which can independently work among S, C, and X bands. The structure of each band is designed separately, and the working frequency can be selected by active switches. To reduce the overall size, the filter uses stacking technology and vertical feedlines to combine each part. Moreover, doubling resonance suppressions are applied in S band by the stepped-impedance resonator to achieve enhanced passband isolation. The designed filter has three passbands at 2.09–3.77 GHz, 3.95–7.25, and 7.78–11.2 GHz, respectively. The simulated results have excellent agreement with the fabricated ones. The proposed work has promising applications in microwave communication scenarios that need higher isolations of working bands.**

***Index Terms*—Active switch, bandpass filter (BPF), doubling resonance, stepped-impedance resonator.**

I. Introduction

THE bandpass filters (BPFs) are widely used in the front end of RF and microwave communication systems. Although the traditional BPFs have excellent performances in the fixed frequency band, they are unable to meet the needs of modern multi-target bands in one component [1], [2], [3], [4], [5], [6]. With the development of 5G technology, the reconfigurable BPFs with higher integration and multiple functional bands are becoming highly attractive.

Recently, varactors are used as one of the electric adjustment methods to shift the working bands of the continuous adjustable BPFs [7], [8], [9], [10], [11], but the ranges of bands need to be expanded. Then, another kind of switchable BPFs was demonstrated which could form different resonant networks to reach larger dynamic ranges of working bands by the ON/OFF states of p-i-n diodes. Commercial switchable filters with high isolations using metal cavities had the problem of difficult integration [12], [13]. To realize the miniaturization of the planar size, four BPFs are vertically stacked on the silicon substrate to achieve frequency band switching in [14]. The multi-layer design suppressed the interaction between the RF path and the bias circuit while achieving miniaturization [15]. Most multi-layer structures generally used microelectromechanical systems (MEMs) or low-temperature cofired ceramic (LTCC) processes [16], [17], which resulted in high costs. An ultra-wide/wideband switching filter was introduced to achieve larger passband isolation by lowpass units [18], but the planar layout occupied a significant amount of space. The multi-mode resonator was used to improve selectivity while achieving miniaturization [19]. However, the out-of-band suppressions were lack of considerations, which may limit the application on the wideband systems. The band-stop filter was cascaded with BPF to obtain additional transmission zeros to improve out-of-band suppression in [20], but the bias network was complex. In [21], a compact dual-band switching filter was realized by using a half-mode substrate integrated waveguide which could shift between S and C bands, but the size of the cavity structure was still large.

This letter proposes a compact triple-band active switchable BPF, in which bandpass performances are realized by interdigital resonators. The core concept of this design is to establish three channels connected to S, C, and X bandpass structures at the common input/output ports, and then utilize the corresponding conduction of bias voltage-controlled p-i-n diodes to switch among channels flexibly. The structures were stacked vertically and fed through the vertical blind via holes (BVHs) for minimization. To enhance the passband isolation, a step-impedance resonator (SIR) was etched in series after the S-band structure to suppress the doubling resonance. Therefore, external suppression in the S-band can reach up to 20 GHz ($6.82f_0$), which could not cause harmonic inferences to the other two bands.

II. Design Theory

A. Analysis of Bandpass Structures and Vertical Feedlines

The stacked structure of the proposed filter is illustrated in Fig. 1. Proposed multi-layer filter. (a) vertical view. (b) lateral view. It consists of five dielectric substrates with a thickness of 300 μm (Sub1 to Sub5) and six copper layers (M1 to M6). RO4003c with a dielectric constant of 3.55 is used as the substrate to further reduce the insertion loss. The bandpass effects for S, C, and X bands are achieved using 7th-order interdigital structures composed of parallel microstrip conductors [Fig. 1(a)]. These conductors create capacitive coupling through electric fields, while the microstrip lines provide inductive properties. Each pair of adjacent conductors forms a resonant unit, with energy transfer facilitated by coupling effects, generating the bandpass

Received 26 February 2025; accepted 23 March 2025. This work was supported in part by the Graduate Innovation Program of China University of Mining and Technology under Grant 2024WLJCRCZL134 and in part by the Postgraduate Research and Practice Innovation Program of Jiangsu Province under Grant SJCX24_1386. *(Corresponding author: Lei Zhao.)*

Ruofeng Xu, Wenhan Wu, Xianglin Kong, Jun Wang, and Lei Zhao are with the School of Information and Control Engineering, China University of Mining and Technology, Xuzhou 221116, China (e-mail: leizhao@cumt.edu.cn).

Yunze Hu and Guoqing Pan are with Beijing Aerospace Measurement and Control Technology Company Ltd., Beijing 100041, China.

Digital Object Identifier 10.1109/LMWT.2025.3554867

2771-957X © 2025 IEEE. All rights reserved, including rights for text and data mining, and training of artificial intelligence and similar technologies. Personal use is permitted, but republication/redistribution requires IEEE permission.
See https://www.ieee.org/publications/rights/index.html for more information.

Authorized licensed use limited to: CHINA UNIVERSITY OF MINING AND TECHNOLOGY. Downloaded on May 19,2025 at 23:34:28 UTC from IEEE Xplore. Restrictions apply.

This article has been accepted for inclusion in a future issue of this journal. Content is final as presented, with the exception of pagination.

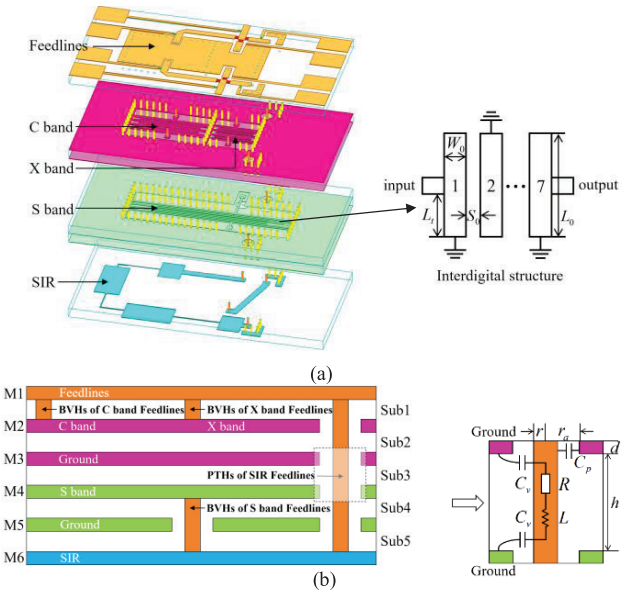

Fig. 1. Proposed multi-layer filter. (a) Vertical view. (b) Lateral view.

TABLE I

STRUCTURE SIZE TABLE (UNIT: MM)

w	w_s	l_s	l_{st}	c_{s_1}	c_{s_2}	c_{s_3}	c_{s_4}	d_{s_1}
0.63	0.17	15.45	9.80	0.05	2.49	2.35	2.39	0.09
d_{s_3}	w_c	l_c	l_{ct}	c_{t_1}	c_{t_2}	c_{t_3}	c_{t_4}	d_{c_1}
0.15	0.30	7.39	3.77	0.04	0.75	0.82	0.81	0.04
d_{c_3}	w_x	l_x	l_{xt}	c_{x_1}	c_{x_2}	c_{x_3}	c_{x_4}	d_{x_1}
0.06	0.24	4.28	1.83	0.05	0.43	0.42	0.41	0.09
d_{x_3}	l_1	l_2	l_3	l_4	l_5	w_l	w_h	
0.15	2.10	4.51	4.67	4.79	2.51	2.41	0.08	

response. The length (L_0) is typically a quarter-wavelength to resonate at the target frequency, while the spacing (S_0) controls coupling strength and bandwidth. The width (W_0) influences characteristic impedance matching and in-band insertion loss. Feedlines are implemented via tapped lines on the outermost units, with positions (L_t) optimized for impedance matching. Geometric parameters are fine-tuned in the high-frequency structure simulator (HFSS) to optimize center frequency and bandwidth, achieving the desired bandpass responses for S, C, and X bands. All parameters are detailed in Table I.

In this design, all bands are fed by vertical vias and the parasitic effect of the via becomes a major challenge in vertical feeding technology. Fig. 1(b) shows the equivalent circuit of the via in one layer. Here, R can be ignored due to the excellent conductivity of vias. The capacitance between each layer is C_v, the coaxial capacitance is C_p, and C is the parasitic capacitance, $C = C_v + C_p$. C_p can be solved by the electrostatic field. To facilitate the equivalence, L and C_p can be estimated by the following equation:

$$L = 5.08h\left[\ln\frac{4h}{r} + 1\right], \quad C_p = \frac{2\pi\varepsilon_r\varepsilon_0}{\ln\frac{r_a}{r}} \tag{1}$$

where h and r are the height and radius of the via, respectively. ε_0 and ε_r are the dielectric constant of air and the relative

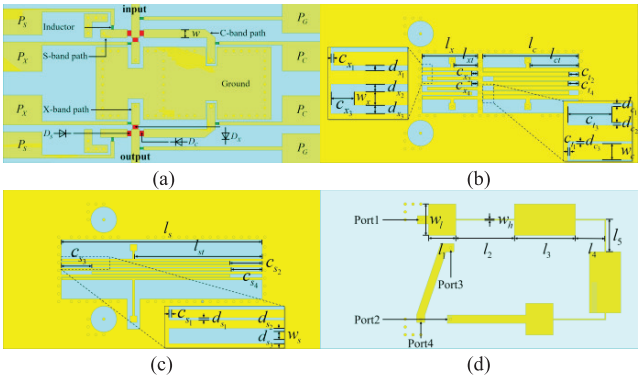

Fig. 2. (a) Top view of the feedline layer. (b) Top view of C, X-band layer. (c) Top view of S-band layer. (d) Top view of the SIR layer.

TABLE II

CONDITIONS OF THE BAND SELECTION

Band selection	Bias pad connection (Positive voltage level)	Diode status (on/off)
S	Ps(connected); Pc, Px(disconnected)	Ds(on); Dc, Dx(off)
C	Pc(connected); Ps, Px(disconnected)	Dc(on); Ds, Dx(off)
X	Px(connected); Ps, Pc(disconnected)	Dx(on); Ds, Dc(off)

dielectric constant of the dielectric, r_a is the radius of the via pad. If the via is divided into v segments, the interlayer capacitance C_v is

$$C_v = \frac{2\pi\varepsilon_r\varepsilon_0}{\ln\frac{r_a}{r}} \cdot \sum_{p=1}^{v} \frac{(h+d)(r_a - r)}{v\sqrt{\left(\frac{h}{2} - (p-1)\left(\frac{h}{2v}\right)\right) + (r_a - r)^2}}. \tag{2}$$

When h is constant, L can be reduced by the increase of r. If r is similar to r_a, C_v will become quite large to generate severe parasitic capacitance effects. Thus, due to the limited size of via pad, r should be as small as possible to reach the limit of machining accuracy. Eventually, by choosing the appropriate aperture, the diameters of vertical feeding lines for S, C, and X-band are chosen as 0.2, 0.3, and 0.3 mm, respectively.

B. Switching Mechanism and Design of the Stacked Structure

Feedlines with the dc biased network are set at M1 and the bias directions of p-i-n diodes are shown in Fig. 2(a). Six p-i-n diodes (MADP-000907-14020 with series resistance 5.2 Ω) are etched in each channel at the input/output 50 Ω ports, which are fed by the microstrip line to ground coplanar waveguide (GCPW). The diodes are controlled by four pairs of pads in the dc bias networks. P_Gs are consistently connected to the negative voltage level, while Ps, Pc, and Px are linked to the positive level. Band selection is determined by which diodes are activated via the bias pads to establish the input/output channel. Inductors are positioned before each diode to prevent electromagnetic signals from interfering with the dc source. Table II outlines the switching mechanism based on the diodes' ON/OFF states.

Three different bands of BPFs are realized at the M2 and M4 layers and are stacked by pressing a PP sheet RO4450F with a dielectric constant of 3.52. To ensure the isolation of adjacent circuits in the vertical direction, an electromagnetic shielding metal cavity is formed by plating through holes (PTHs) and

Authorized licensed use limited to: CHINA UNIVERSITY OF MINING AND TECHNOLOGY. Downloaded on May 19,2025 at 23:34:28 UTC from IEEE Xplore. Restrictions apply.

This article has been accepted for inclusion in a future issue of this journal. Content is final as presented, with the exception of pagination.

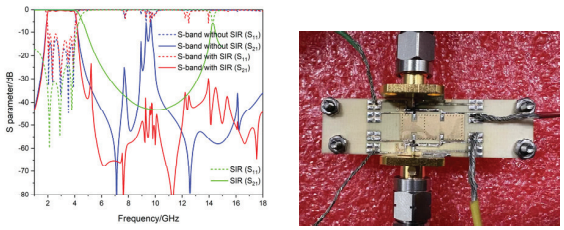

(a) (b)

Fig. 3. (a) Frequency responses of SIR and S-band with/without SIR. (b) Prototype with dc bias.

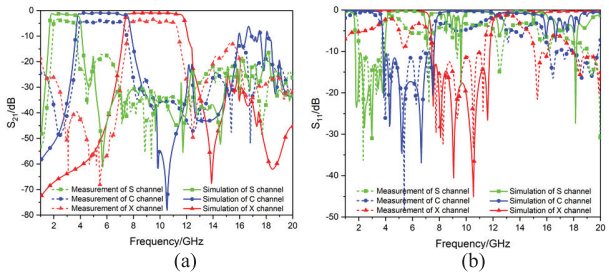

(a) (b)

Fig. 4. *S*-parameter results. (a) $|S_{21}|$. (b) $|S_{11}|$.

metal ground planes (M3, M5). In Fig. 2(b), the left rectangular part is an X-band bandpass structure, and the right one is a C-band bandpass structure. To improve the external quality factor, all bandpass structures are fed by tapped lines, which are connected to BVHs as feedlines. The S-band bandpass structure is set at M4 and the top view is shown in Fig. 2(c). The SIR layer is at M6. The size of the laminated filter is $24.464 \times 12.2 \times 1.71$ mm. All bandpass structures are constructed vertically in sealed metal cavities to reduce the spatial scattering, which can be considered as striplines with higher effective dielectric constant to achieve compact unit size.

C. Realization of Enhanced Passband Isolation

The S-band interdigital structure induces harmonic resonances at C and X bands, which can disrupt filtering environments requiring sensitive passband isolation. To address this, the SIR layer integrates a series of microstrip lines with varying widths and directly connects to the S-band at M6. The high-impedance segments function akin to series inductors, and the low-impedance segments resemble shunt capacitors, collectively establishing a low-pass filter. The SIR's cutoff frequency is strategically set at 4 GHz to mitigate S-band harmonic resonance. Opting for a 7th-order configuration [Fig. 2(d)] bolsters out-of-band selectivity and diminishes insertion loss. Design constraints limit the high-impedance segments to 0.08 mm (100 Ω) and the low-impedance ones to 2.41 mm (20 Ω). The lengths of these stepped impedance lines are calculated based on the low-pass prototype filter's normalized values and characteristic impedances. The resultant SIR frequency responses, depicted in Fig. 3(a), exhibit an effective lowpass under 4 GHz.

As shown in Fig. 2(d), port 1 and port 4 are connected to M1 through PTH, and port 2 and port 3 are connected to M5 through BVHs. The position of the metal hole ensures that the input signals pass through the SIR and S-band structure sequentially, and then output from the M1. Fig. 3(a) shows that the resonance occurs at 7.7–10 GHz if there is no SIR connected. It can be greatly eliminated by the SIR, while the bandpass performance is still maintained at S-band.

III. Measurement and Results

The prototype was fabricated by multi-layer PCB process and shown in Fig. 3(b). The fabricated filter was measured by the vector network analyzer 3672C. The series protection resistance of each diode was 1.2 kΩ, the forward bias voltage was set to 5 V, and the current value was about 4 mA.

TABLE III
Comparison With Other Works

REF.	Range (GHz)	IL (dB)	Fabrication Technology	>15dB Stopband up to	Size (λ_g^2)
[14]	7.8-9.6/8.2-9.9/9.2-10.9/10.2-11.9	4.2-5.2	3-D TSV-MEMS	/	0.5 × 0.25
[15]	2.8-3.3/3.8-4.2	2.2-3.8	PCB	/	0.78 × 0.86
[18]	3.25-6.05/2.15-11.85	1.6	PCB	$3.86f_0$	0.80 × 0.42
[19]	0.46-0.82/1.37-1.71/2.22-2.7	4-5	PCB	$3f_0$	0.29 × 0.26
[20]	1-1.5/1.5-2/2-2.5/2.5-3	1.5-3.8	PCB	$2.91f_0$	0.34 × 0.29
This work	**2.09-3.77/3.95-7.25/7.78-11.2**	**3.28-4.78**	**PCB**	$6.82f_0$	**0.24 × 0.12**

The *S*-parameter comparisons of the measured and simulated results are shown in Fig. 4(a) and (b). It indicates that the proposed filter can provide excellent bandpass performance in S/C/X-band independently with dynamic switches. Harmonic doubling resonance was greatly reduced by the integrated SIR. The S-band has a wide out-of-band suppression, which can reach 20 GHz ($6.82f_0$). In each passband, measured insertion losses are less than 4.78 dB, and return losses are greater than 10.8 dB. The BWs of the three channels are 1.6 (55%)/3.3 (58%)/3.4 (35%) GHz. Compared with the simulation results, the bandwidths of S/C/X bands decrease by 0.4/0.6/0.6 GHz. This was due to the limitation of the minimum line spacing (>100 μm) in PCB processing, which made the physical line spacing a little larger. The insertion losses were mainly caused by the resistors of diodes and the roughness of the fabrication technology.

Table III summarizes the comparisons with other works, where f_0 refers to the center frequency of the lowest frequency band. It reveals that this design has the advantage of wider switching coverage with a larger isolation range. The design has a more compact size by using the stacked PCB technology, which also greatly reduces the processing cost and difficulty.

IV. Conclusion

This letter demonstrates a switchable filter with a miniaturized design through multi-layer stacking, vertical feedlines, and cross-coupled resonators. The flexible switching among S, C, and X-band can be achieved by diode-controlled channels. Meanwhile, the low-pass SIR is cascaded to achieve broadband external suppression, and the structure exhibits excellent passband isolation in a wide frequency range. The proposed filter is expected to be applied on the tuning RF front end of communication systems which need isolated working bands.

Authorized licensed use limited to: CHINA UNIVERSITY OF MINING AND TECHNOLOGY. Downloaded on May 19,2025 at 23:34:28 UTC from IEEE Xplore. Restrictions apply.

This article has been accepted for inclusion in a future issue of this journal. Content is final as presented, with the exception of pagination.

REFERENCES

[1] S. Yan et al., "A terahertz band-pass filter based on coplanar-waveguide and spoof surface plasmon polaritons," *IEEE Photon. Technol. Lett.*, vol. 34, no. 7, pp. 375–378, Apr. 1, 2022.

[2] Z. Yue, K. Ma, and Y. Wang, "Design of Ka-band SISL high selectivity bandpass filter with controllable zeros," *IEEE Microw. Wireless Technol. Lett.*, vol. 33, no. 9, pp. 1278–1281, Sep. 2023.

[3] W. Tang, R.-F. Xu, and L. Zhao, "A miniaturized C-B and SIW bandpass filter based on LTCC," *Appl. Comput. Electromagn. Soc. J. (ACES)*, vol. 38, pp. 741–745, Feb. 2024.

[4] M. Malki, L. Yang, and R. Gómez-García, "Triple-passband channelized passive filter with infinite input-quasi-reflectionless range," *IEEE Microw. Wireless Technol. Lett.*, vol. 33, no. 5, pp. 519–522, May 2023.

[5] R. F. Xu, W. Tang, X. L. Kong, J. Wang, and L. Zhao, "Miniaturized bandpass filter based on slot perturbation," *Chin. J. radio Sci.*, vol. 38, no. 3, pp. 485–490, 2023.

[6] J. Wang, L. Zhao, and Z.-C. Hao, "A band-pass filter based on the spoof surface plasmon polaritons and CPW-based coupling structure," *IEEE Access*, vol. 7, pp. 35089–35096, 2019.

[7] H. Yang et al., "Spoof surface plasmon polariton-based continuously tunable cutoff frequency filter," *IEEE Microw. Wireless Technol. Lett.*, vol. 33, no. 10, pp. 1430–1433, Oct. 2023.

[8] Z. Chen, K. Ma, Y. Wang, N. Yan, and K. Wang, "A quad-operation-mode tunable SISL bandpass filter with compact size and self-packaging," *IEEE Microwave Wireless Technol. Lett.*, vol. 33, no. 4, pp. 379–382, Apr. 2023.

[9] B.-W. Xu, S. Y. Zheng, and W. Che, "Flexible tri-band coupler with three independently tunable frequencies," *IEEE Trans. Microw. Theory Techn.*, vol. 72, no. 9, pp. 5441–5454, Mar. 2024.

[10] Q. Li and T. Yang, "Compact UWB half-mode SIW bandpass filter with fully reconfigurable single and dual notched bands," *IEEE Trans. Microwave Theory Techn.*, vol. 69, no. 1, pp. 65–74, Jan. 2021.

[11] Y. Hou et al., "A 935–953 MHz Q-enhanced CMOS tunable bandpass filter with ultra-narrowband and ultralow power for RFID applications," *IEEE Trans. Microw. Theory Techn.*, vol. 72, no. 10, pp. 6120–6129, Oct. 2024.

[12] K. Y. Chan, R. Ramer, and R. R. Mansour, "*Ku*-band channel aggregation waveguide filters by RF MEMS-based detuning," *IEEE Trans. Microw. Theory Techn.*, vol. 68, no. 2, pp. 750–761, Nov. 2019.

[13] T. R. Jones and M. Daneshmand, "Miniaturized folded ridged quarter-mode substrate integrated waveguide RF MEMS tunable bandpass filter," *IEEE Access*, vol. 8, pp. 115837–115847, 2020.

[14] F. Hou et al., "Micropackaged compact switchable filters with high isolation in 3-D TSV-MEMS process," *IEEE Trans. Compon., Packag., Manuf. Technol.*, vol. 11, no. 4, pp. 647–654, Apr. 2021.

[15] Z. Yan et al., "A high-performance dual-band switchable bandpass filter and its application in 5G signal detector," *IEEE Trans. Compon., Packag., Manuf. Technol.*, vol. 13, no. 8, pp. 1242–1253, Aug. 2023.

[16] K. Kageyama, K. Saito, H. Murase, H. Utaki, and T. Yamamoto, "Tunable active filters having multilayer structure using LTCC," *IEEE Trans. Microw. Theory Techn.*, vol. 49, no. 12, pp. 2421–2424, Dec. 2001.

[17] E. Arabi, F. A. Ghaffar, and A. Shamim, "Tunable bandpass filter based on partially magnetized ferrite LTCC with embedded windings for SoP applications," *IEEE Microw. Wireless Compon. Lett.*, vol. 25, no. 1, pp. 16–18, Jan. 2015.

[18] A. Bandyopadhyay, P. Sarkar, and R. Ghatak, "A bandwidth reconfigurable bandpass filter for ultrawideband and wideband applications," *IEEE Trans. Circuits Syst. II, Exp. Briefs*, vol. 69, no. 6, pp. 2747–2751, Jun. 2022.

[19] M.-E. Tian, Z.-H. Long, L.-J. Feng, L.-L. He, and T.-L. Zhang, "Switchable and tunable triple-channel bandpass filter," *Chin. Phys. B*, vol. 31, no. 7, Jun. 2022, Art. no. 078401.

[20] C. Liu, Y. Rao, Z. Deng, W. Li, and X. Luo, "Marshaling access: Four-channel switchable filter bank," *IEEE Microw. Mag.*, vol. 21, no. 1, pp. 73–81, Jan. 2020.

[21] R. Xu, W. Tang, J. Wang, and L. Zhao, "A compact bandpass filter with active switchable passband status," *Appl. Comput. Electromagn. Soc. J.*, vol. 38, no. 9, pp. 746–750, Feb. 2024.

Authorized licensed use limited to: CHINA UNIVERSITY OF MINING AND TECHNOLOGY. Downloaded on May 19,2025 at 23:34:28 UTC from IEEE Xplore. Restrictions apply.